This article has been accepted for publication in a future issue of this journal, but has not been fully edited. Content may change prior to final publication. Citation information: DOI 10.1109/TCSII.2021.3088942, IEEE Transactions on Circuits and Systems II: Express Briefs

An L_1-norm based Optimization Method for Sparse Redundancy Resolution of Robotic Manipulators

Zhan Li and Shuai Li

***Abstract*—For targeted motion control tasks of manipulators, it is frequently necessary to make use of full levels of joint actuation to guarantee successful motion planning and path tracking. Such way of motion planning and control may keep the joint actuation in a non-sparse manner during motion control process. In order to improve sparsity of joint actuation for manipulator systems, a novel motion planning scheme which can optimally and sparsely adopt joint actuation is proposed in this paper. The proposed motion planning strategy is formulated as a constrained L_1 norm optimization problem, and an equivalent enhanced optimization solution dealing with bounded joint velocity is proposed as well. A new primal dual neural network with a new solution set division is further proposed and applied to solve such bounded optimization which can sparsely adopt joint actuation for motion control. Simulation and experiment results demonstrate the efficiency, accuracy and superiority of the proposed method for optimally and sparsely adopting joint actuation. The average sparsity (i.e., -$\|\dot{\theta}\|_p$ where θ denotes the joint angle) of the joint motion of the manipulator can be increased by 39.22$\%$ and 51.30$\%$ for path tracking tasks in X-Y and X-Z planes respectively, indicating that the sparsity of joint actuation can be enhanced.**

***Index Terms*—Redundancy resolution, dynamic neural network, kinematic control, sparsity**

I. Introduction

In recent years, various manipulators have emerged to facilitate humans to help improve their work efficiency and quality of life [1], [2]. The solution for inverse kinematics is a fundamental issue to find proper joint actuation configuration to fulfill end-effector manipulation tasks before utilization of operability of manipulators. However, strong coupled nonlinearity always exists in the mapping between a joint space and a Cartesian workspace of a manipulator. It is rather difficult to handle this problem by obtaining analytical solutions in the joint space level through directly solving the coupled nonlinear equations which are used to describe the kinematic characteristics of manipulators. Therefore, the kinematic control problem in the joint space is converted into a problem at a joint velocity level.

Some early works reveal the kinematic control solutions can be directly obtained by solving the pseudoinverse of the Jacobian matrix of a manipulator without any physical constraints. Such way of processing may lead to unexpected local instability and even need more computational costs which are not afforded, but it still suffers from the drawback of neglecting additional necessary performance indices (e.g., joint limits or task-oriented constraints) with unexpected computational burdens. Applying recurrent neural networks to solve motion planning with additional optimization requirement can be a promising route to achieve excellent optimization performance for accurate motion control of manipulators [3], [4], [5]. For instance, in [6], discrete zeroing neural network models were reformulated as an equality-constrained quadratic programming to perform kinematic control of manipulators. In [7], an adaptive projection neural network was utilized to control the manipulator with unknown physical parameters and have shown promising tracking performance. In [8], the mobile manipulator's time-varying disturbances could be elegantly suppressed by a robust zeroing neural-dynamics.

Towards accurate motion control of manipulators for adopting joint actuation in a sparse manner, it may be a feasible way to propose a sparse redundancy resolution for manipulators in the level of joint angular velocity. To achieve such goal, the designed redundancy resolution scheme for manipulators is supposed to be formulated as an L_1-norm based sparse optimization paradigm. However, currently there is almost no related work on an L_1-norm based sparse redundancy resolution for manipulators. Motivated by these points, different from conventional L_2-norm based redundancy resolution paradigms [9], [10], [11] for kinematic control of manipulators in a non-sparse manner, this paper aims to make breakthroughs by proposing a redundancy resolution method which is able to sparsely and optimally modulate joint actuation, and a primal dual neural network for such sparsity-based resolution scheme is developed. The contributions of this brief are summarized as follows. 1) This brief proposes an L_1-norm based sparse redundancy resolution method for kinematic control of manipulators with joint limits. 2) A new primal dual neural network with a new solution set is proposed for the L_1-norm based sparse redundancy resolution with additional bounded joint velocity. 3) Both simulation and experiment results demonstrate the efficiency of the proposed L_1-norm based redundancy resolution for the manipulator with the sparsity of the joint motion enhanced.

II. Proposed Sparse Redundancy Resolution of Manipulators

In this section, inspired by L_1-norm based sparse paradigms in signal processing [12], [13], [14], we propose to formulate the sparse redundancy resolution of the manipulator into the L_1-norm based optimization problem.

This work was supported by the Sichuan Key Research and Develop Project under Grant 2021YFS0067. *(Corresponding author: Shuai Li.)*

Z. Li is with School of Automation Engineering, University of Electronic Science and Technology of China, Chengdu 611731, China. Z. Li is affiliated with the Computer Science Department, Swansea University, Swansea, UK. (Email: zhan.li@uestc.edu.cn).

S. Li is with College of Engineering, Swansea University, Swansea, UK. (e-mail: shuai.li@swansea.ac.uk).

This article has been accepted for publication in a future issue of this journal, but has not been fully edited. Content may change prior to final publication. Citation information: DOI 10.1109/TCSII.2021.3088942, IEEE Transactions on Circuits and Systems II: Express Briefs

A. L_1-based Optimization for Redundancy Resolution

In this brief, the following L_1 norm ($\|\cdot\|_1$) based optimization for redundancy resolution is proposed:

$$\begin{aligned} \text{minimize} \quad & \|\dot{\theta}\|_1 \\ \text{subject to} \quad & J\dot{\theta} = \dot{r}_d \\ & \dot{\theta} \in \Omega = \{\eta^- \leq \dot{\theta} \leq \eta^+\}. \end{aligned} \tag{1}$$

where θ denotes the joint angle variable of the manipulator, J denotes the Jacobian matrix, r_d denotes the desired path of the end-effector, η^- and η^+ receptively denote the lower and upper limits of joint velocity.

It is worth mentioning here that, L_0-norm based optimization is not strictly convex and can be seen as a NP-hard computational problem, and thus L_1-norm based optimization is chosen as the sparse alternative to remedy the weakness of using L_0-norm based paradigm. As the velocity kinematics equation is acting as a constraint on joint velocity rather than joint angle or acceleration, the proposed sparse optimization is focusing on joint velocity resolution and can be utilized for velocity feedback control.

In order to solve the optimization problem (1), we need to firstly define the following Lagrange function:

$$L = \|\dot{\theta}\|_1 + \lambda^T(J\dot{\theta} - \dot{r}_d) \tag{2}$$

where $\lambda \in R^3$ denotes the Lagrange multiplier vector.

By differentiating the Lagrange function above with respect to $\dot{\theta}$ and λ, we have the following group of equations:

$$\begin{cases} \frac{\partial L}{\partial \dot{\theta}} = J^T\lambda + \frac{\partial \|\dot{\theta}\|_1}{\partial \dot{\theta}} = J^T\lambda + \text{sgn}(\dot{\theta}) \\ \frac{\partial L}{\partial \lambda} = J\dot{\theta} - \dot{r}_d \end{cases} \tag{3}$$

where $\text{sgn}(\dot{\theta}) = [\text{sgn}(\dot{\theta}_1), \text{sgn}(\dot{\theta}_2), \cdots, \text{sgn}(\dot{\theta}_n)]^T$ with

$$\text{sgn}(\dot{\theta}_i) = \begin{cases} 1, & \text{if } \dot{\theta}_i > 0 \\ 0, & \text{if } \dot{\theta}_i = 0 \\ -1, & \text{if } \dot{\theta}_i < 0 \end{cases}$$

According to the design principle of primal dual neural network [15], [16], the corresponding primal dual neural network for solving (1) is constructed as follows:

$$\begin{cases} \epsilon\ddot{\theta} = -\dot{\theta} + P_\Omega(\dot{\theta} - \frac{\partial L}{\partial \dot{\theta}}) \\ \epsilon\dot{\lambda} = J\dot{\theta} - \dot{r}_d \end{cases} \tag{4}$$

where $\epsilon > 0$ denotes the parameter to scale the convergence, and $P_\Omega(\cdot)$ denotes the linear piecewise projection function with the solution set Ω, i.e.,

$$P_\Omega(z) = \begin{cases} z^+, z > z^+ \\ z, z^- \leq z \leq z^+ \\ z^-, z < z^- \end{cases}. \tag{5}$$

Due to the existence of $\text{sgn}(\dot{\theta})$ which is not smooth, the primal dual neural network solver (4) may encounter unexpected computation difficulties in the solution process and has degraded convergence performance, so it is not a good alternative for solving optimization problem (1) to achieve the sparse redundancy resolution. In order to remedy this, we propose to reformulate the optimization problem (1) in the ensuring subsection.

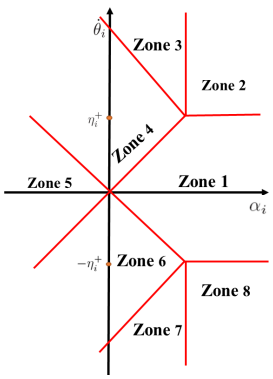

Zone 1	$\lvert\dot{\theta}_i\rvert \leq \eta_i^+$ and $\lvert\dot{\theta}_i\rvert \leq \alpha_i$
Zone 2	$\dot{\theta}_i \geq \eta_i^+$ and $\alpha_i \geq \eta_i^+$
Zone 3	$\alpha_i \leq \eta_i^+$ and $\dot{\theta}_i \geq -\alpha_i + 2\eta_i^+$
Zone 4	$\dot{\theta}_i \geq \lvert\alpha_i\rvert$ and $\dot{\theta} \leq -\alpha + 2\eta_i^+$
Zone 5	$\lvert\dot{\theta}_i\rvert \leq -\alpha_i$
Zone 6	$\dot{\theta}_i \leq -\lvert\alpha_i\rvert$ and $\dot{\theta}_i \geq \alpha_i - 2\eta_i^+$
Zone 7	$\alpha_i \leq \eta_i^+$ and $\dot{\theta}_i \leq \alpha_i - 2\eta_i^+$
Zone 8	$\dot{\theta}_i \leq -\eta_i^+$ and $\alpha_i \geq \eta_i^+$

Fig. 1. The partition of $(\alpha_i, \dot{\theta}_i)$ plane to construct projection $P_{\overline{\Omega}_i}(\cdot)$.

B. Enhanced Solution with Bounded Joint Velocity

To make the optimization problem (1) solved by the primal dual neural network, we equivalently propose a new optimization formulation:

$$\begin{aligned} \text{minimize} \quad & h^T\alpha \\ \text{subject to} \quad & J\dot{\theta} = \dot{r}_d \\ & \dot{\theta} \in \overline{\Omega} \end{aligned} \tag{6}$$

where $h^T = [1, 1, \cdots, 1]$, $\alpha^T = [\alpha_1, \alpha_2, \cdots, \alpha_n]$, and a new solution set $\overline{\Omega} = \{\dot{\theta} \in \Omega \text{ and } -\alpha \leq \dot{\theta} \leq \alpha\}$ is defined. Optimization formulation (6) is the general optimization paradigm which is ready to solve the L_1-norm based sparse optimization problem (1) with bounded joint velocity, through additionally introducing the variable α to restrict the joint velocity $\dot{\theta}$ simultaneously. Under the circumstances, the joint velocity variable possess a preset boundary $\eta^- \leq \dot{\theta} \leq \eta^+$ and a dynamic limit $-\alpha \leq \dot{\theta} \leq \alpha$.

In order to solve optimization problem (6), we have to define the following Lagrange function for such enhanced formulation:

$$L = h^T\alpha + \lambda^T(J\dot{\theta} - \dot{r}_d). \tag{7}$$

By differentiating the Lagrange function above with respect to the unknown variables $\dot{\theta}$, α and λ, we would get the following group of equations:

$$\begin{cases} \frac{\partial L}{\partial \dot{\theta}} = J^T\lambda \\ \frac{\partial L}{\partial \alpha} = h \\ \frac{\partial L}{\partial \lambda} = J\dot{\theta} - \dot{r}_d \end{cases}. \tag{8}$$

According to the aforementioned design procedure of the primal dual neural network for solving optimization problems, we can have the following new primal dual neural network solver for the sparse optimization of redundancy resolution:

$$\begin{cases} \epsilon \begin{bmatrix} \ddot{\theta} \\ \dot{\alpha} \end{bmatrix} = -\begin{bmatrix} \dot{\theta} \\ \alpha \end{bmatrix} + P_{\overline{\Omega}}\left(\begin{bmatrix} \dot{\theta} \\ \alpha \end{bmatrix} - \begin{bmatrix} \frac{\partial L}{\partial \dot{\theta}} \\ \frac{\partial L}{\partial \alpha} \end{bmatrix} \right) \\ \epsilon\dot{\lambda} = J\dot{\theta} - \dot{r}_d \end{cases} \tag{9}$$

where the solution set cone $\overline{\Omega} = \bigcup_{i=1}^n \overline{\Omega}_i$ with boundaries $\eta_i^- \leq \dot{\theta}_i \leq \eta_i^+$ and $-\alpha_i \leq \dot{\theta}_i \leq \alpha_i$.

This article has been accepted for publication in a future issue of this journal, but has not been fully edited. Content may change prior to final publication. Citation information: DOI 10.1109/TCSII.2021.3088942, IEEE Transactions on Circuits and Systems II: Express Briefs

For the properties of the newly-proposed linear piecewise projection function $P_{\overline{\Omega}}(\cdot)$ with the new divided solution set $\overline{\Omega}$, we have

$$P_{\overline{\Omega}}\left(\begin{bmatrix}\dot{\theta}\\ \alpha\end{bmatrix}\right)=\bigcup_{i=1}^{n}P_{\overline{\Omega}_i}\left(\begin{bmatrix}\dot{\theta}_i\\ \alpha_i\end{bmatrix}\right) \tag{10}$$

and its subparts can be expanded as follows:

$$P_{\overline{\Omega}_i}\left(\begin{bmatrix}\dot{\theta}_i\\ \alpha_i\end{bmatrix}\right)=\begin{cases}\begin{bmatrix}\dot{\theta}_i\\ \alpha_i\end{bmatrix}, |\dot{\theta}_i|\le\eta_i^+ \text{ and } |\dot{\theta}_i|\le\alpha_i\\ \begin{bmatrix}\eta_i^+\\ \alpha_i\end{bmatrix}, \dot{\theta}_i\ge\eta_i^+ \text{ and } \alpha_i\ge\eta_i^+\\ \begin{bmatrix}-\eta_i^+\\ \alpha_i\end{bmatrix}, \dot{\theta}_i\le-\eta_i^+ \text{ and } \alpha_i\ge\eta_i^+\\ \begin{bmatrix}\eta_i^+\\ \eta_i^+\end{bmatrix}, \alpha_i\le\eta_i^+ \text{ and } \dot{\theta}_i\ge-\alpha_i+2\eta_i^+\\ \begin{bmatrix}-\eta_i^+\\ \eta_i^+\end{bmatrix}, \alpha_i\le\eta_i^+ \text{ and } \dot{\theta}_i\le\alpha_i-2\eta_i^+\\ \begin{bmatrix}(\dot{\theta}_i+\alpha_i)/2\\ (\dot{\theta}_i+\alpha_i)/2\end{bmatrix}, |\alpha_i|\le\dot{\theta}_i\le-\alpha_i+2\eta_i^+\\ \begin{bmatrix}(\dot{\theta}_i-\alpha_i)/2\\ (-\dot{\theta}_i+\alpha_i)/2\end{bmatrix}, \alpha_i-2\eta_i^+\le\dot{\theta}_i\le-|\alpha_i|\\ \begin{bmatrix}0\\ 0\end{bmatrix}, |\dot{\theta}_i|\le-\alpha_i\end{cases} \tag{11}$$

with its new divided solution sets in the $(\alpha_i,\dot{\theta}_i)$ plane shown in Fig. 1. So the linear piecewise projection operator $P_{\overline{\Omega}_i}(\cdot)$ is based on the divided solution set $\overline{\Omega}_i$ to guarantee the convergence of the optimization solver. As compared with previous works [15], [16], this paper proposes a new linear piecewise projection function with a new solution set $\overline{\Omega}$. The new solution set $\overline{\Omega}$ expands the original divided three solution subsets with five more new ones.

C. Enhanced Solution without Joint Velocity Bounds

If the joint velocity bound $\dot{\theta}\in\Omega=\{\eta^-\le\dot{\theta}\le\eta^+\}$ is not involved for the aforementioned enhanced optimization formulation, the solution set $\overline{\Omega}$ reduces to another new solution set $\widetilde{\Omega}$. Thus the correspondingly the optimization problem (6) reduces to

$$\begin{aligned}\text{minimize}\quad & h^T\alpha\\ \text{subject to}\quad & J\dot{\theta}=\dot{r}_d\\ & \dot{\theta}\in\widetilde{\Omega}.\end{aligned} \tag{12}$$

The primal dual neural network solver (9) can be utilized to solve optimization problem (12) with the new solution set $\widetilde{\Omega}$, and the corresponding linear piecewise projection function for such a solution set cone $\widetilde{\Omega}$ is

$$P_{\widetilde{\Omega}_i}\left(\begin{bmatrix}\dot{\theta}_i\\ \alpha_i\end{bmatrix}\right)=\begin{cases}\begin{bmatrix}\dot{\theta}_i\\ \alpha_i\end{bmatrix}, |\dot{\theta}_i|\le\alpha_i\\ \begin{bmatrix}(\dot{\theta}_i+\alpha_i)/2\\ (\dot{\theta}_i+\alpha_i)/2\end{bmatrix}, \dot{\theta}_i\ge|\alpha_i|\\ \begin{bmatrix}0\\ 0\end{bmatrix}, |\dot{\theta}_i|\le-\alpha_i\\ \begin{bmatrix}(\dot{\theta}_i-\alpha_i)/2\\ (-\dot{\theta}_i+\alpha_i)/2\end{bmatrix}, \dot{\theta}_i\le-|\alpha_i|\end{cases} \tag{13}$$

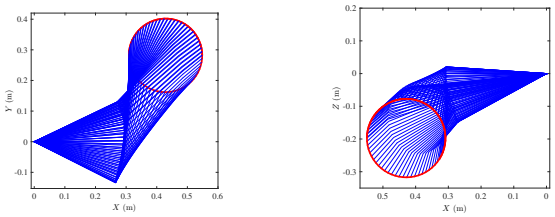

(a) X-Y plane (b) X-Z plane

Fig. 2. Circle path tracking performance in X-Y and X-Z planes of the manipulator synthesised by the proposed motion control method which uses part of the actuators.

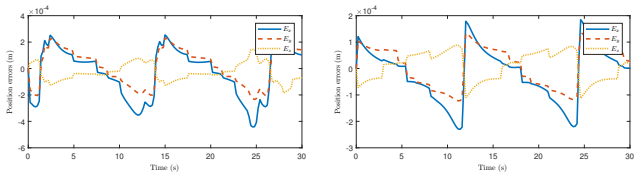

(a) In X-Y plane (b) In X-Z plane

Fig. 3. Position errors of the end point of the manipulator for tracking the desired circle path in X-Y and $X-Z$ planes by the proposed sparse optimization method.

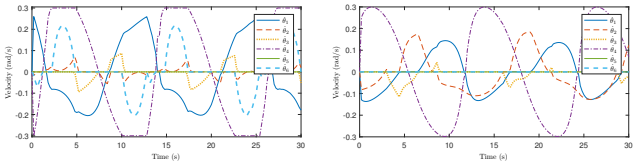

(a) In X-Y plane (b) In X-Z plane

Fig. 4. Joint velocity of the manipulator resolved by the proposed method in X-Y and X-Z planes, the joint velocity is limited by the set bounds.

Comparing the linear piecewise projections $P_{\overline{\Omega}_i}(\cdot)$ and $P_{\widetilde{\Omega}_i}(\cdot)$, we can easily see that involvement of the joint velocity bounds can make the solution set cone with more boundary lines to divide the phase plane (α_i,η_i). Optimization (12) without joint velocity bounds can be regarded as the special case of optimization (6) with joint velocity bounds.

III. Results

A. Simulation Verification

In the simulation, the desired end-effector motion is configured as a circle planned in X-Z and X-Y planes with its radius being 0.12 m. The radius of the targeted circle path has to be constrained by the manipulability index $\sqrt{\det(J^TJ)}$ to preserve the reachability under fixed mechanism parameters in the D-H table of the manipulator. The joint velocity bounds for the manipulator is set as -0.3 rad/s and 0.3 rad/s.

1) Path Tracking: Fig. 2 shows the generated trajectory by the proposed method. In this figure, the piecewise straight lines in blue represent the body of the manipulator, and the curves in red represent the trajectory of the end-point/effector. It can be obviously seen that the generated trajectories of the manipulator successfully both track the desired circle path.

Furthermore, Fig. 3 shows the position errors of the end-point/end-effector of the manipulator for tracking the desired

This article has been accepted for publication in a future issue of this journal, but has not been fully edited. Content may change prior to final publication. Citation information: DOI 10.1109/TCSII.2021.3088942, IEEE Transactions on Circuits and Systems II: Express Briefs

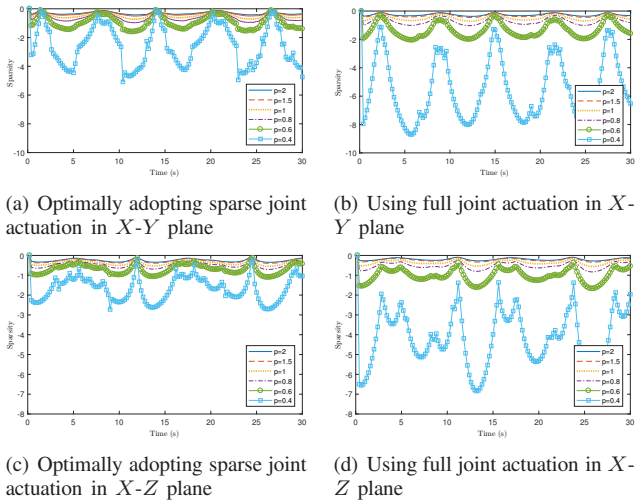

(a) Optimally adopting sparse joint actuation in X-Y plane

(b) Using full joint actuation in X-Y plane

(c) Optimally adopting sparse joint actuation in X-Z plane

(d) Using full joint actuation in X-Z plane

Fig. 5. Sparsity evaluation of the joints of the manipulator for motion control in X-Y and X-Z planes.

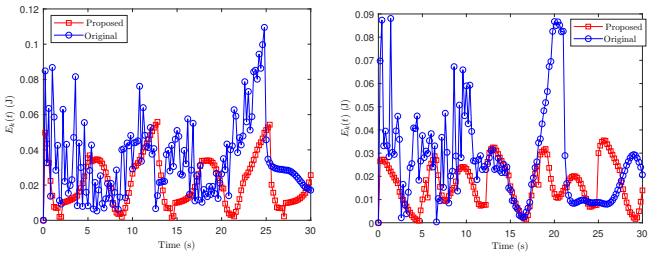

(a) Kinetic energy comparison in X-Y plane

(b) Kinetic energy comparison in X-Z plane

Fig. 6. Comparisons on the kinetic energy of the links between the proposed method and the method without sparse optimization.

circle path synthesised by the proposed method, and we could evidently see that the errors can be reached to a level of 4×10^{-4} m in X-Y plane and a level of 3×10^{-4} m in X-Z plane. These results show that, the accuracy of the motion control for the manipulator model can be guaranteed by the proposed sparse optimization method. As compared with the results reported in previous works [15], [16], the motion planning and control results in this work can achieve the same level of tracking accuracy for the end-effector/end-point of the manipulator. Fig. 4 shows the joint angular velocity resolution by the proposed sparse optimization method in both X-Y and X-Z planes. From Fig. 4(a), we can evidently see that, for the motion control task in X-Y plane, joint velocity of Joint 5 is always turned down, joint velocity of Joint 2 is almost turned down during the whole motion process, and actuation of Joint 3 and Joint 6 is turned down in some time periods (e.g., around 0 s-5 s and 10 s-17.5 s for Joint 3, around 4.5 s-10 s and 17 s-20 s for Joint 6). For the motion control task in X-Z plane shown in Fig. 4(b), we can see that joint velocity of Joint 5 and Joint 6 is turned down during the whole motion process, joint velocity of Joint 1 and Joint 3 is turned down in some time period (e.g., around 3 s-7 s and 16 s-19 s for Joint 1, around 8 s-16 s and 17 s-29 s for Joint 3). Reviewing the circle path tracking performance in Fig. 2 and Fig. 3, we conclude that, with optimally adopting the joint actuation by the proposed method, the circle path tracking task can still be fulfilled with promising position error performance, although some joints' velocities are turned down for some periods.

2) Sparsity Evaluation: Joint sparsity comparisons are made with and without the proposed method. The sparsity metric is computed by the aforementioned index $-\|\dot{\theta}\|_p$. Fig. 5 shows the comparisons of sparsity metric $-\|\dot{\theta}\|_p$ ($p = 2, 1.5, 1, 0.8, 0.6, 0.4$) with optimally adopting sparse joint actuation and with using full joint actuation based on the method in [16] which are without sparse optimization for circle path tracking in both X-Y and X-Z planes. From the figure, we can see that, after optimally adopting sparse joint actuation by the proposed method, the sparsity is enhanced promisingly, especially when $p = 0.4$ is set. Table I quantitatively shows the computed average sparsity in the two cases. When optimally adopting sparse actuation of joints, the average sparsity metric value is -5.19±2.45 and -3.17±1.27 in X-Y and X-Z planes respectively. Nevertheless, when full actuation is used for all joints, the average sparsity metric value is -8.54±3.34 and -6.51±2.23 in X-Y and X-Z planes respectively. The average sparsity can be increased by around 39.22% and 51.30% in X-Y and X-Z planes respectively. These results indicate that the proposed method can increase the sparsity of joint angles when fulfilling the same circle path tracking task. Fig. 6 shows the comparison results of the total kinetic energy of the links of the manipulator system based on the proposed sparse method in this paper and the method [16], and we can see that the proposed method can achieve lower level of kinetic energy variations.

TABLE I
AVERAGE SPARSITY OF THE MANIPULATOR SYSTEM DURING MOTION CONTROL EXPERIMENTS

Desired path plane for motion control	Optimally adopting sparse actuation joint actuators	Using actuation of all joints
X-Y plane	**-5.19±2.45**	-8.54±3.34
X-Z plane	**-3.17±1.27**	-6.51±2.23

B. Experiment Validation

In the experiment sessions, the tracking paths for the end-effector are respectively set as the circle path with diameter 0.24 m in X-Y plane and X-Z plane. Figs. 7 and 8 show the path tracking performance correspondingly. We could obviously observe that, with utilizing the proposed sparse redundancy resolution scheme, the end-effector/end-point of the manipulator system can keep tracking the desired circle path(s) in both X-Y and X-Z planes well with promising accuracy. Fig. 8 further shows the position errors of the end-effractor/end-point during path tracking tasks in both X-Y and X-Z planes synthesised by the proposed method, we can evidently see that the position errors in three dimensions $[E_x, E_y, E_z]$ are rather small ($< 6 \times 10^{-3}$ m). Fig. 9 shows the joint angles from Joint 1 to Joint 6 i.e., θ resolved by the proposed method in both X-Y and X-Z planes. In X-Y plane, Joint 5's angle is kept constant during the whole motion

This article has been accepted for publication in a future issue of this journal, but has not been fully edited. Content may change prior to final publication. Citation information: DOI 10.1109/TCSII.2021.3088942, IEEE Transactions on Circuits and Systems II: Express Briefs

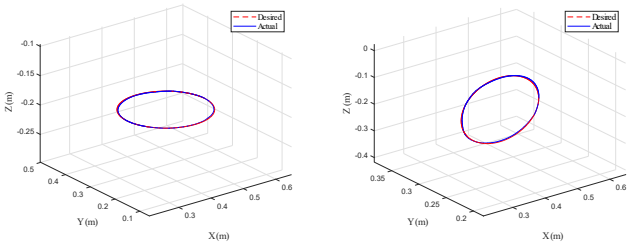

(a) Tracking performance in X-Y plane (b) Tracking performance in X-Z plane

Fig. 7. Experimental path tracking performance in X-Y plane and X-Z plane for the manipulator system.

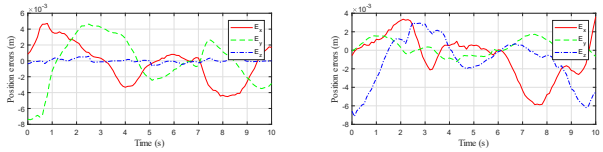

(a) Error performance in X-Y plane (b) Error performance in X-Z plane

Fig. 8. Experimental position tracking errors in X-Y plane and X-Z plane for the manipulator system.

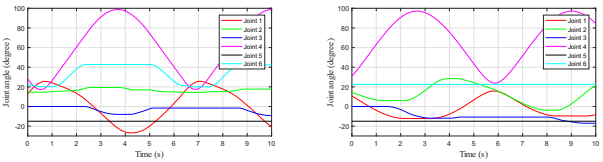

(a) Joint angles in X-Y plane (b) Joint angles in X-Z plane

Fig. 9. Experimental joint angles in X-Y plane and X-Z plane for the manipulator system.

process, the joint angles of Joint 3 and Joint 6 are keeping constant in some periods, and Joint 3's actuation is always kept as a low motion level. In X-Z plane, the actuation of Joint 5 and Joint 6 is off during the whole motion process, the the joint angles of Joint 1 and Joint 3 are keeping constant in some periods. The experiment results demonstrate the efficiency of the proposed L_1-norm based method for motion planning and control together with the low-level servo controller.

IV. Conclusion

In this brief, an L_1-norm based optimization paradigm and a corresponding new primal dual neural network have been proposed for sparse redundancy resolution of manipulators. Simulation and experiment results demonstrate the efficiency, accuracy and superiority of the proposed method with sparsity enhanced. For the future works, the extended works can be developing anti-noise dynamic neural networks [17], [18] for sparse redundancy resolution with robust performances. Moreover, effective algorithms for L_p-norm ($0 \leq p < 1$) based sparse redundancy resolution which is not strictly convex are required to be developed, by integrating sparse representation methods using multivariate Laplace function or multivariate Geman-McClure function [19].

References

[1] G. H. Xu, F. Qi, Q. Lai, and H. H. C. Iu, "Fixed time synchronization control for bilateral teleoperation mobile manipulator with nonholonomic constraint and time delay," *IEEE Transactions on Circuits and Systems II: Express Briefs*, vol. 67, no. 12, pp. 3452–3456, 2020.

[2] J. Zhai and G. Xu, "A novel non-singular terminal sliding mode trajectory tracking control for robotic manipulators," *IEEE Transactions on Circuits and Systems II: Express Briefs*, vol. 68, no. 1, pp. 391–395, 2021.

[3] Z. Zhang and Z. Yan, "A varying parameter recurrent neural network for solving nonrepetitive motion problems of redundant robot manipulators," *IEEE Transactions on Control Systems Technology*, vol. 27, no. 6, pp. 2680–2687, 2019.

[4] Z. Zhang, Y. Lin, S. Li, Y. Li, Z. Yu, and Y. Luo, "Tricriteria optimization-coordination motion of dual-redundant-robot manipulators for complex path planning," *IEEE Transactions on Control Systems Technology*, vol. 26, no. 4, pp. 1345–1357, 2018.

[5] Z. Zhang, T. Fu, Z. Yan, L. Jin, L. Xiao, Y. Sun, Z. Yu, and Y. Li, "A varying-parameter convergent-differential neural network for solving joint-angular-drift problems of redundant robot manipulators," *IEEE/ASME Transactions on Mechatronics*, vol. 23, no. 2, pp. 679–689, 2018.

[6] B. Liao, Y. Zhang, and L. Jin, "Taylor $o(h^3)$ discretization of ZNN models for dynamic equality-constrained quadratic programming with application to manipulators," *IEEE Transactions on Neural Networks and Learning Systems*, vol. 27, no. 2, pp. 225–237, 2016.

[7] Y. Zhang, S. Chen, S. Li, and Z. Zhang, "Adaptive projection neural network for kinematic control of redundant manipulators with unknown physical parameters," *IEEE Transactions on Industrial Electronics*, vol. 65, no. 6, pp. 4909–4920, 2018.

[8] D. Chen and Y. Zhang, "Robust zeroing neural-dynamics and its time-varying disturbances suppression model applied to mobile robot manipulators," *IEEE Transactions on Neural Networks and Learning Systems*, vol. 29, no. 9, pp. 4385–4397, 2018.

[9] Z. Zhang, L. Kong, and L. Zheng, "Power-type varying-parameter rnn for solving tvqp problems: Design, analysis, and applications," *IEEE Transactions on Neural Networks and Learning Systems*, vol. 30, no. 8, pp. 2419–2433, 2019.

[10] Z. Zhang, X. Deng, L. Kong, and S. Li, "A circadian rhythms learning network for resisting cognitive periodic noises of time-varying dynamic system and applications to robots," *IEEE Transactions on Cognitive and Developmental Systems*, vol. 12, no. 3, pp. 575–587, 2020.

[11] Z. Zhang, S. Chen, and S. Li, "Compatible convexcnonconvex constrained qp-based dual neural networks for motion planning of redundant robot manipulators," *IEEE Transactions on Control Systems Technology*, vol. 27, no. 3, pp. 1250–1258, 2019.

[12] A. Jiang, H. K. Kwan, Y. Tang, and Y. Zhu, "Sparse fir filter design via partial 1-norm optimization," *IEEE Transactions on Circuits and Systems II: Express Briefs*, vol. 67, no. 8, pp. 1482–1486, 2020.

[13] B. N. G. Koneru and V. Vasudevan, "Sparse artificial neural networks using a novel smoothed lasso penalization," *IEEE Transactions on Circuits and Systems II: Express Briefs*, vol. 66, no. 5, pp. 848–852, 2019.

[14] J. Yoo, J. Shin, and P. Park, "An improved nlms algorithm in sparse systems against noisy input signals," *IEEE Transactions on Circuits and Systems II: Express Briefs*, vol. 62, no. 3, pp. 271–275, 2015.

[15] D. Guo and Y. Zhang, "A new inequality-based obstacle-avoidance mvn scheme and its application to redundant robot manipulators," *IEEE Transactions on Systems, Man, and Cybernetics, Part C (Applications and Reviews)*, vol. 42, no. 6, pp. 1326–1340, 2012.

[16] S. Li, M. Zhou, and X. Luo, "Modified primal-dual neural networks for motion control of redundant manipulators with dynamic rejection of harmonic noises," *IEEE Transactions on Neural Networks and Learning Systems*, vol. 29, no. 10, pp. 4791–4801, 2018.

[17] L. Xiao, Y. Zhang, Z. Hu, and J. Dai, "Performance benefits of robust nonlinear zeroing neural network for finding accurate solution of lyapunov equation in presence of various noises," *IEEE Transactions on Industrial Informatics*, vol. 15, no. 9, pp. 5161–5171, 2019.

[18] L. Xiao, J. Dai, R. Lu, S. Li, J. Li, and S. Wang, "Design and comprehensive analysis of a noise-tolerant znn model with limited-time convergence for time-dependent nonlinear minimization," *IEEE Transactions on Neural Networks and Learning Systems*, vol. 31, no. 12, pp. 5339–5348, 2020.

[19] G. Wang, C. Yang, and X. Ma, "A novel robust nonlinear kalman filter based on multivariate laplace distribution," *IEEE Transactions on Circuits and Systems II: Express Briefs*, pp. 1–1, 2021.